Aerosol Science and Technology

ISSN: (Print) (Online) Journal homepage: www.tandfonline.com/journals/uast20

Air cleaner prototype: Reduction of airborne viruses and effects of UV-C irradiation on virus concentration and RNA copy numbers considering modeled residence times and doses

Jochen Schulz, Vivian Natascha Lochte, Sebastian Blessing, Alexander Stroh, Jochen Kriegseis, Nicole Kemper, Martin Limbach & Horst Hahn

To cite this article: Jochen Schulz, Vivian Natascha Lochte, Sebastian Blessing, Alexander Stroh, Jochen Kriegseis, Nicole Kemper, Martin Limbach & Horst Hahn (28 Oct 2024): Air cleaner prototype: Reduction of airborne viruses and effects of UV-C irradiation on virus concentration and RNA copy numbers considering modeled residence times and doses, Aerosol Science and Technology, DOI: 10.1080/02786826.2024.2412633

To link to this article: https://doi.org/10.1080/02786826.2024.2412633

Published online: 28 Oct 2024.

AEROSOL SCIENCE AND TECHNOLOGY
https://doi.org/10.1080/02786826.2024.2412633

Air cleaner prototype: Reduction of airborne viruses and effects of UV-C irradiation on virus concentration and RNA copy numbers considering modeled residence times and doses

Jochen Schulz[a], Vivian Natascha Lochte[a], Sebastian Blessing[b], Alexander Stroh[b], Jochen Kriegseis[b], Nicole Kemper[a], Martin Limbach[c], and Horst Hahn[c*]

[a]Institute for Animal Hygiene, Animal Welfare and Farm Animal Behaviour, University of Veterinary Medicine Hannover, Foundation, Hannover, Germany; [b]Institute of Fluid Mechanics, Karlsruhe Institute of Technology, Karlsruhe, Germany; [c]Institute of Nanotechnology, Karlsruhe Institute of Technology, Karlsruhe, Germany

ABSTRACT

A prototype of an air cleaner was investigated for its ability to inactivate airborne MS2 viruses *via* UV-C irradiation. AGI-30 impingers were used to measure virus concentrations and RNA copy numbers at the air cleaner's inlet and outlet, which was integrated into a testing system. UV-C doses were estimated by modeling the viruses' dwell times in the device and measuring the UV-C radiance level. The appliance reduced infectious viruses by 99% to 92% in airflows ranging from 113 to 153 m^3/h, with the reduction rate decreasing as airflow increased. Estimated UV-C doses ranged between 2.11 and 2.95 mWs/cm^2. There was a significant correlation between the virus reduction and corresponding doses (Spearman $\rho = 0.77$, $p = 0.0092$; Kendall's $\tau = 0.60$, $p = 0.0157$). Modeling showed that assuming laminar flows or air exchange rates would overestimate the viral particles' residence time in the device. Measurements indicated that viral particles remained partly trapped in the device, and RNA copy numbers did not correlate with the number of infectious viruses. RNA copy number concentrations were up to 3.7 log units above plaque-forming units (PFU) levels (for non-irradiated samples) and reduced only by 19% following UV-C exposure. This discrepancy could be attributed to the RT-PCR used, which also detects RNA fragments from incomplete or noninfectious virus particles. The mismatch between RNA copy detection and the number of infectious viruses raises questions about the appropriateness of using nucleic acid copy numbers for risk assessments or modeling.

GRAPHICAL ABSTRACT

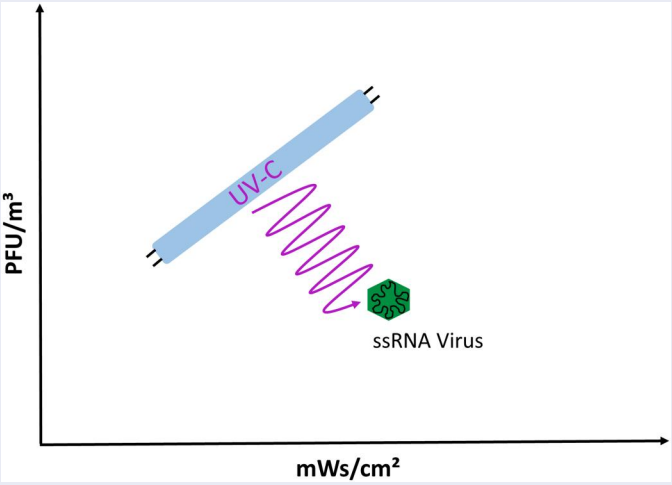

ARTICLE HISTORY
Received 25 March 2024
Accepted 8 September 2024

EDITOR
Shanna Ratnesar-Shumate

CONTACT Jochen Schulz jochen.schulz@tiho-hannover.de Institute for Animal Hygiene, Animal Welfare and Farm Animal Behaviour, Bischofsholer Damm 15, 30173 Hannover, Germany, University of Veterinary Medicine Hannover, Foundation, Hannover, Germany.
*Current affiliation: University of Oklahoma, School of Sustainable Chemical, Biological and Materials Engineering, Normal, Oklahoma, USA

Introduction

The SARS-CoV-2 pandemic has significantly increased the demand for air purifiers, which operate on various principles. The airborne transmission of the virus in indoor settings is undeniable, and using air purifiers – either standalone ones in rooms or those integrated into ventilation systems – is a recommended strategy for curbing the risk of infection (Shen et al. 2021). Among the options available, filtration systems and UV irradiation systems are widely used for both public facilities and for homes (Szczotko et al. 2022).

Numerous studies have outlined the effectiveness of UV-C irradiation in eliminating airborne bacteria, viruses, molds, and yeasts (Kowalski 2010). However, research on the efficiency of commercial UV-C air purifiers is scarce, which could be useful to manufacturers, vendors – as a selling point – and customers who desire assurance of efficacy.

A testing technique for evaluating the performance of air purifiers against airborne viruses involves the use of surrogate viruses. These surrogate viruses are less dangerous compared to pathogenic ones, thus enabling investigations to take place in lower-level biosafety labs, such as BSL 1 or 2. The phage MS2 is often chosen as a surrogate for small airborne viruses and can be used to assess the inactivation of airborne viruses by UV-C irradiation (Beswick et al. 2023).

Although studies on MS2 can deliver insights applicable to pathogenic viruses, it is important to note that UV-C dosage required to inactivate 90% of MS2 is likely higher than that needed for SARS-CoV-2 but has also been reported to be lower than influenza viruses in some studies. (e.g., Allen, Benner, and Bahnfleth 2021).

A variety of systems have been utilized to detect airborne viruses in field samples (Bhardwaj et al. 2021; Cox et al. 2020). However, not every bioaerosol sampling method is effective for assessing virus concentrations in ventilation ducts, especially when operating within a virus-enriched air stream. This circumstance leads to contamination of the devices and complicates the sample exchange process. In this instance, stack sampling methods may prove more beneficial. The AGI-30 Impinger and the Andersen sampler, for example, have been employed for stack sampling to detect live microorganisms or active viruses (Jensen 1964; Walker and Ko 2007; Yang et al. 2018). Sampler inlets can be linked to a duct *via* tubes or probes. Moreover, filtration, washing or reincorporation of particles back into the ducts can control particles that have not been collected and have been re-aerosolized from the outlet of the samplers. This control is of particular importance when the equipment setup cannot be positioned in a chamber that can protect from released aerosols.

Walker and Ko (2007) studied the impact of UV-C irradiation on airborne MS2 phages using AGI-30 impingers. The study, conducted within a biological safety cabinet, evaluated UV-C's effect on various airborne viruses, particularly the phage MS2, using a pre-determined dosage. This dosage only inactivated a portion of MS2. However, the dosages needed for significant 90% (D_{90} value) and 99% (D_{99} value) inactivation are a key consideration in the creation of UV-C-based air purifiers (Kowalski 2010; Montalli et al. 2021).

In another study, survival rates were measured by an Andersen sampler in a system with an airflow rate of 3.6 m^3 per hour. The researchers calculated 0.3 to 0.4 mWs/cm^2 and 0.8 to 0.9 mWs/cm^2 dosages are required to inactivate 90% and 99% of airborne MS2, respectively (Tseng and Li 2008). Other authors cited a requirement of 1.2 mWs/cm^2 for the D_{90} value of airborne MS2 (Allen, Benner, and Bahnfleth 2021).

Certain factors such as test conditions, particle sizes, detection methods, and UV susceptibility influence the data on airborne viruses, making comparisons between studies a difficult task (Abkar et al. 2022). Moreover, practical aspects must be considered when assessing the efficiency of a UV-C device. For instance, the device design might impact particle flow uniformity, and cause turbulence or electrostatic precipitation. This might assist the reduction of airborne viruses but would overestimate the efficiency at a certain UV-C dose.

Other influencing parameters, such as airflow rate and the duration airborne viruses remain within the irradiated section, also determine the dose. Hence, efficiency outcomes that consider these variables could provide beneficial information for both the designers and users of the devices.

This study sought to assess the ability of a prototype UV-C device, designed to decrease airborne viruses in enclosed spaces, by using airborne surrogate MS2 viruses. The device was integrated into a test system that facilitated virus collection at both the apparatus's inlet and outlet, employing a stack sampling method across various air volumes. We simulated the residence times of virus particles in the device and computed UV-C doses. Additionally, the ongoing pandemic highlighted the significance of RNA copy numbers in examining airborne virus transmission (Buonanno et al. 2022). Consequently, this study included the detection of RNA copy numbers as well.

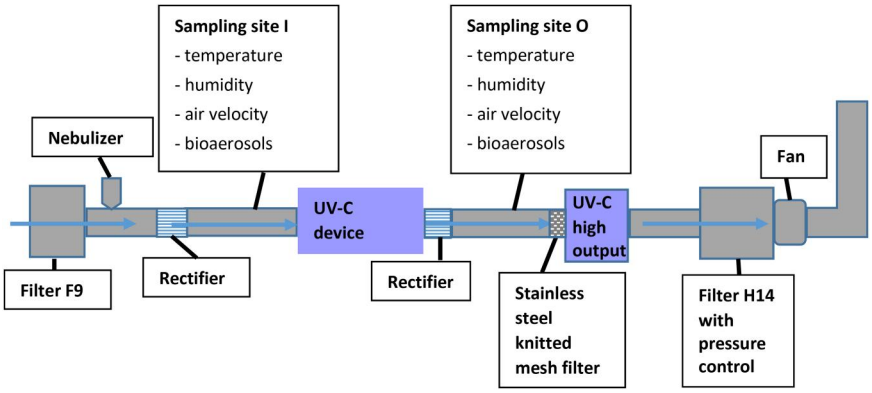

Figure 1. Test system to analyze the reduction of airborne viruses through an integrated UV-C device (prototype).

Material and methods

Test system

Figure 1 presents a test system schematic that includes the embedded UV-C device. At the sample sites temperature, humidity, and air velocity were measured using the Testo 400 instrument (Testo SE & Co. KGaA, Lenzkirch, Germany). The system's interconnected devices utilized circular tubes with a cross-section of 0.01227 m^2. The system's fan (S&P Deutschland GmbH, Darmstadt, Germany) was adjustable, achieving a maximum velocity of 3.6 m/s in the tubes when at full power, which is equivalent to a maximum flow rate of 159 m^3/h. The intake air was initially filtered with a F9 Filter (ISO 16890 classification: ePM1 filter, with 80% efficiency for particles ranging from 0.3–1 µm) to prevent the room air's potential airborne bacteria from contaminating the surrogate viruses' growth medium and causing disruptions in detection. To eliminate the test viruses from the expelled air, UV-C radiation was applied in a high-output section carrying two low-pressure mercury lamps (254 nm) (TUV 55 W LL lamps, UV-Technik Speziallampen GmbH, Ilmenau, Germany) behind the sampling site O. Per the manufacturer's statement, the radiation flow of both lamps was 36 $W_{UV\text{-}C}$. At the inlet of the section a stainless steel knitted mesh filter is incorporated to avoid additional UV-C reflections at sampling site O. UV-C irradiance was not detectable behind this filter (<0.05 mW/cm^2) by the UV-C sensor SI 1 (A002072, uv-technik meyer gmbh, Ortenberg, Germany). The output air finally passed through a H14 filter (with a minimum 99.995% particle filtration efficiency for 0.3 µm particles). The UV-C prototype device was located between two rectifiers that minimize the turbulence at the sample locations. This prototype device was equipped with two low-pressure mercury lamps (ozone free, 254 nm) linked to the test system with welded flanges and rubber sleeves. Not equipped with its own fan, it relied on the test system for air supply.

Virus production and nebulization

We used the single-stranded (+) RNA coliphage MS2 virus (ATCC 15597-B1) as surrogate virus. Following Uhde et al. (2022) protocol with minor modifications, the virus was propagated and purified in *Escherichia coli* (ATCC 23631), abiding by ISO 10705-173 standards. We prepared a large virus stock and preserved it at 4 °C. Fresh 1:100 dilutions were made using sterile deionized water.

Subsequently, this suspension was administered into a medical nebulizer (PARI BOY® Pro. PARI GmbH, Weilheim, Germany) for each of the 20 trials. To quantify the viral concentration in the nebulized suspensions, an immediate sample was obtained from the nebulizer before each sampling commenced. The viral concentration was appraised *via* the plaque-forming units (PFU) count obtained through plaque assay method, as described in source (Uhde et al. 2022).

The plaque assay involved the propagation of phages using a two-layer agar overlay procedure. The bottom agar layer was made using tryptone-yeast extract-glucose agar (TYGA). Meanwhile, the upper semi-solid agar layer mixed with a calcium-glucose solution was combined with 1 ml of bacterial culture (in the logarithmic growth phase) and 1 ml of freshly prepared suspensions for nebulizing. After pouring this mixture over the bottom layer, the plates were incubated at 37 °C for 20 h, and the PFU was recorded.

Each measurement involved operating the nebulizer filled with freshly prepared phage suspension for 15 min. The amount of nebulized phages ranged from approximately 1.5×10^9 to 4.4×10^9 PFU.

Sampling of airborne viruses and RNA copies

Stack sampling was executed at the I and O sites using identical circular stainless steel probes with a

0.009 m inner diameter, concurring with the inlet size of the sampling devices (Impinger, AGI-30, LAT, Garbsen, Germany). The probes were curved at a 90-degree angle to face the airflow. They connected to the impinger *via* sterilized silicon tubes. Before establishing the connection, the impingers were filled with 30 ml of sterile PBS buffer.

The impingers' outlets are linked to a gas-washing bottle containing a 30% glycerol and 70% ethanol solution aimed at purifying the air of phages. Rotameters (Analyt-MTC, Müllheim, Germany) placed between the gas wash bottle outlet and plunger pumps adjusted and regulated the flow rates.

Flow rates were adjusted to match the different volumes: 10 l/min at volumes ranging from 111 to 114 m^3/h, 11 l/min at volumes from 120 to 123 m^3/h, 12 l/min at volumes from 135 to 137 m^3/h, 13 l/min at volumes from 144 to 147 m^3/h, and 14 l/min at volumes from 157 to 161 m^3/h. This configuration resulted in a near-uniform air velocity in the tubes, sampling probes, and impinger inlets (isokinetic sampling).

Air sampling at I and O sites ran for 15 min parallel to the virus suspension nebulization process. We undertook four measurements at each of five sampling days: two trials with UV-C exposure and two without, in alternating order. Before samples were taken with UV-C, lamps were turned on 20-min prior to sampling. Overall, 20 samples were taken from I and 20 samples were taken simultaneously from O (10 with and 10 without UV-C irradiation). Due to variations in the recorded air velocities, calculated air volumes differed up to 4 m^3/h between the four trials at one day. Day one (111, 113, 114 and 112 m^3/h), day two (122, 122, 120 and 123 m^3/h), day three (136, 135, 138 and 137 m^3/h), day four (146, 144, 146 and 147 m^3/h) and day five (161, 157, 159 and 158 m^3/h).

The mean room air temperature upon entering was $23.3\,^{\circ}C \pm 1.3\,^{\circ}C$ with relative humidity at 52.1% ± 4.8%. UV-C treatment induced an increase in temperature to $26.3\,^{\circ}C \pm 1.3\,^{\circ}C$ as the relative humidity dropped to 44.6% ± 4.2%.

After the day's sampling, the entire system was disinfected. To achieve this, an ozone generator was positioned facing the box (F9 filter). We adjusted the air velocity to 1 m/s and let the generator produce 10,000 mg of ozone per hour. The proceeding 60 min involved a thorough gas-flushing of the system. The calculated ozone concentration was 226.2 mg/m^3. The resulting dose (13,560 min (mg/m^3) is sufficient to inactivate more than 99% of DNA and RNA viruses (including MS2) on surfaces and reduces RNA copies below the detection limit (Tseng and Lee 2008; Volkoff et al. 2021).

Quantification of airborne viruses and RNA copy numbers

To determine the remaining volume of the sample buffer post-sampling, the impingers filled with it were weighed prior to and post-sampling. At room temperature, the density of the PBS buffer stands at 1.0, making 1 g equal to 1 ml. Subsequent to sampling, a serial dilution was assembled using 1 ml of the sampling buffer. 1 ml from the dilutions was then mixed with 1 ml of the *E. coli* propagation strain in the top layer. The samples underwent incubation as described earlier, and PFU were counted from decimal dilutions resulting in 35-350 plaques. In cases of two countable plates from consecutive dilutions, the weighted mean was calculated for PFU/ml. Finally, Equation (1) was used to compute the concentration per cubic meter.

$$\frac{PFU}{m^3} = \frac{PFU}{V_{plated\ \ aliquote}[ml]} \times \frac{dilution\ \ factor \times V_{buffer\ \ after\ \ sampling}\ [ml]}{V_{air\ \ sample}\ [m^3]} \tag{1}$$

The RNA copy numbers from PCR samples were calculated using a calibration curve produced from RNA extracted from the stock solution of the virus. The RNA extraction was conducted using the QIAamp Viral RNA Mini Kit (Qiagen, Hilden, Germany) according to the manufacturer's protocol. RNA concentration from both the virus stock suspension and air samples was measured photometrically utilizing a BioDrop Duo + spectrophotometer (BioDrop, UK). A calibration line (Figure 2) was generated using a serial dilution of the extracted RNA from the stock (96.54 µg/ml). The reverse transcription PCR (RT-PCR) process was carried out in line with Dreier, Störmer, and Kleesiek (2005), except for the fluorescence marker used. The fluorescence marker (CY5) and quencher (BHQ2) were attached to the probe in this sequence: CY5-

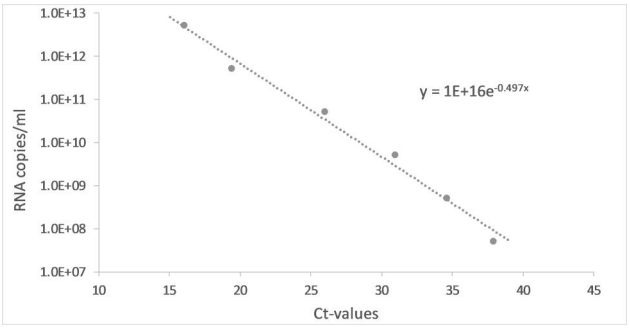

Figure 2. Calibration line to calculate the RNA copy numbers from air samples by One-Step RT-PCR.

ACCTCGGGTTT CCGTCTTGCTCGT-BHQ2. Probes were designed by Eurofins Genomics Germany GmbH. PCR was performed using the SUPERSCRIPT III One-Step RT-PCR with PLATINUM Taq kit (Fisher Scientific GmbH, Schwerte, Germany). The cycle thresholds (Ct) were determined thrice for each dilution, and the average Ct value was plotted against the RNA copies/ml (Figure 2). The number of RNA copies per ml of each dilution was estimated using the molecular weight of the MS2 RNA molecule (1147411.8 g/mol), the initial RNA concentration measured from the virus stock, and the corresponding dilution factor. The calibration line equation in Figure 2 was employed to quantify airborne RNA copy numbers using the Ct-values measured from impinger sample buffers.

Modeling residence times of particles and doses at different flow rates

To calculate the UV-C doses to which viruses were exposed at different air flows, the times spent in the device's irradiated channels were modeled *via* flow simulations. These simulations relied on OpenFOAM-7 (Weller et al. 1998), an open-source software. For this process, the geometry of the device prototype was illustrated (Figure 3). Subsequently, a computational mesh was made using the simplified geometry, employing the meshing utility of the Siemens StarCCM + software package. This mesh is unstructured and incorporates added prism layers to enhance computational precision in areas near the wall. It consists of approximately 1.5 million polyhedral cells.

The Navier-Stokes solver *pimpleFoam*, a solver for transient, incompressible problems based on the combined PISO and SIMPLE algorithms for pressure coupling, was used to compute the velocity and pressure fields for five different flow rates (100, 150, 200, 250 and 300 $\frac{m^3}{h}$), resulting in a Reynolds number range of $Re \approx [12,000; 37,000]$ based on the hydraulic diameter of an irradiated channel.

The k-ω-SST model was chosen to model turbulent effects due to its good performance and robustness in wall-bounded internal turbulent flow (Menter, Kuntz, and Langtry 2003). Boundary conditions for the turbulence model were estimated using best practices (OpenCFD Limited 2021) with an assumed inlet turbulence intensity of $Tu = 10\%$ and a mixing length of $l = 24\ mm$. The kinematic viscosity of air was approximated as $\nu = 10^{-5}\frac{m^2}{s}$. Gravitational effects were neglected. Adaptive time-stepping has been used with the convergence condition limited by $Co < 0.3$. The boundary conditions chosen for the simulations are denoted in Table 1. Each simulation was run for $t = 10\ s$ of physical time on 80 CPUs. The results were visualized using ParaView (Ahrens et al. 2005).

To calculate the residence times, we seeded particles in the inlet area of the device, as shown by the green surface in Figure 3a, utilizing ParaViews' StreamTracer utility. We then traced these particles through the velocity field by integrating the path line equation (Spurk and Aksel 2020)

$$\overrightarrow{u} = \mathrm{d}\overrightarrow{x}/\mathrm{d}t \tag{2}$$

with a time step chosen sufficiently small so no particle skips mesh cells. The integration was stopped when the particle crossed the outlet of the second irradiated channel (the blue surface in Figure 3a) or a fixed amount of time steps that amount to a residence time of $t_{residence} > 3s$ is surpassed. The total physical time

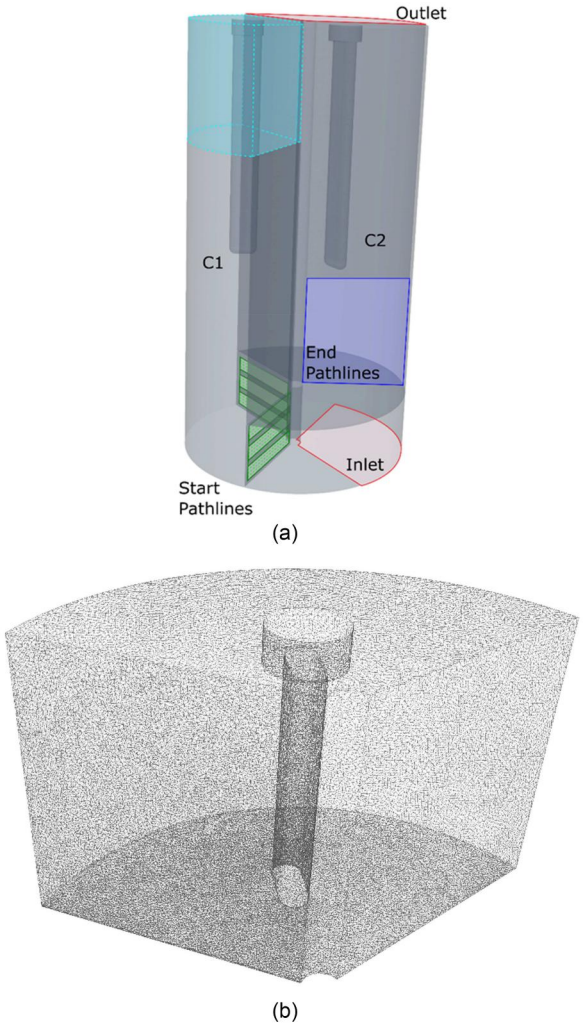

Figure 3. (a) Simplified geometry of the device with starting and end surfaces for path lines. The light green dashed lines in the starting area of the pathlines indicate the seeding lines. (b) Wireframe of a segment of the mesh. The area shown is indicated in light blue in (a).

Table 1. Boundary conditions for velocity U, pressure p, turbulent kinetic energy k and dissipation rate ω as used for the pimpleFoam-based URANS simulations.

Boundary Patch	U	p	k	ω
Inlet	fixed value	zero gradient	fixed value	fixed value
Outlet	zero gradient	fixed value	zero gradient	zero gradient
Walls	no slip	zero gradient	wall function	wall function

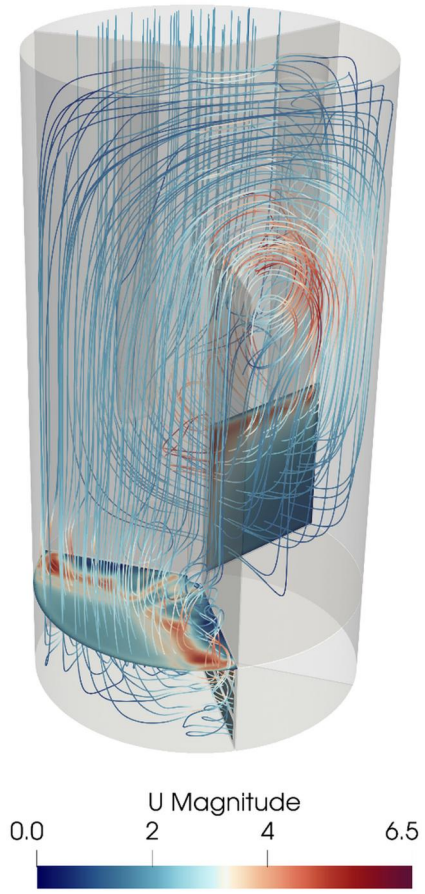

Figure 4. Pathlines of particles in the device at $\dot{V} = 100\,\frac{m^3}{h}$. Color visualizes local velocity [m/s].

required for the particles to reach the terminating surface was deemed the particle's residence time in the irradiated section of the device. It is important to note that the complete time integration at each seeding time was conducted on a consistent, unchanging snapshot of the velocity field at that point in time.

Particles were evenly distributed across 18 lines within the six inlet slits at ten distinctive, nonspecific starting times. This was done to ensure the time between each seeding burst exceeded the average residence time of a particle within the device. Consequently, approximately 110,000 particles were traced throughout the device for each velocity. A sample result is shown in Figure 4 for the flow rate of $\dot{V} = 100\,\frac{m^3}{h}$.

The modeled residence times were utilized to compute the residence times corresponding to varying airflows under test conditions. These times were then multiplied by the UV-C irradiance to estimate the doses absorbed by the viruses when they passed through the device (Equation (3)). The UV-C irradiance was gauged by a sensor (SI 1, A002072, uv-technik meyer gmbh, Ortenberg, Germany) at three different points, namely the beginning, middle and end, along the irradiated channel as well as the UV-C irradiators. The sensor was set in the exterior wall of the channel, with the photodetector aimed toward the centrally located UV lamp in the channel. The distances from the sensor to the lamp were approx. 5 cm at the beginning and the middle of the channel and approx. 8 cm at the end. Measurements were taken under room temperature conditions and with the fan operating. Prior to each measurement, the UV lamps were preheated until there was no increase in irradiance. The average irradiance detected at the three points was considered the minimum irradiance because the distance between the sensor points and the centrally positioned UV lamp roughly corresponds to the greatest distance a particle can have from the irradiator.

Statistics

Data was processed using Excel 2016 (Microsoft Corporation, Redmond, WA, USA). The UNIVARIATE procedure, the CORR procedure, and the TTEST procedure were used for data analysis in SAS 9.4 (SAS Institute, Cary, NC, USA). Plots were generated with sgplot.

Results

Figure 5 presents the concentrations recorded at both the inlet (I) and the outlet (O) of the device, corresponding to different air flows and UV-C irradiation states. RNA copy numbers were three to four logs higher than PFU. While RNA copy numbers did not exhibit any consistent trends between positions I and O, PFU O was consistently lower than PFU I. This implies a PFU loss as the viruses traversed the system. This reduction was more pronounced with UV-C activation. However, the concentration of cultivable viruses after irradiation (PFU O UV) tended to increase with higher air flows. Moreover, when UV-C was on, the RNA copy number was typically lower at the outlet (RNA copies O UV) compared to the inlet (RNA copies I).

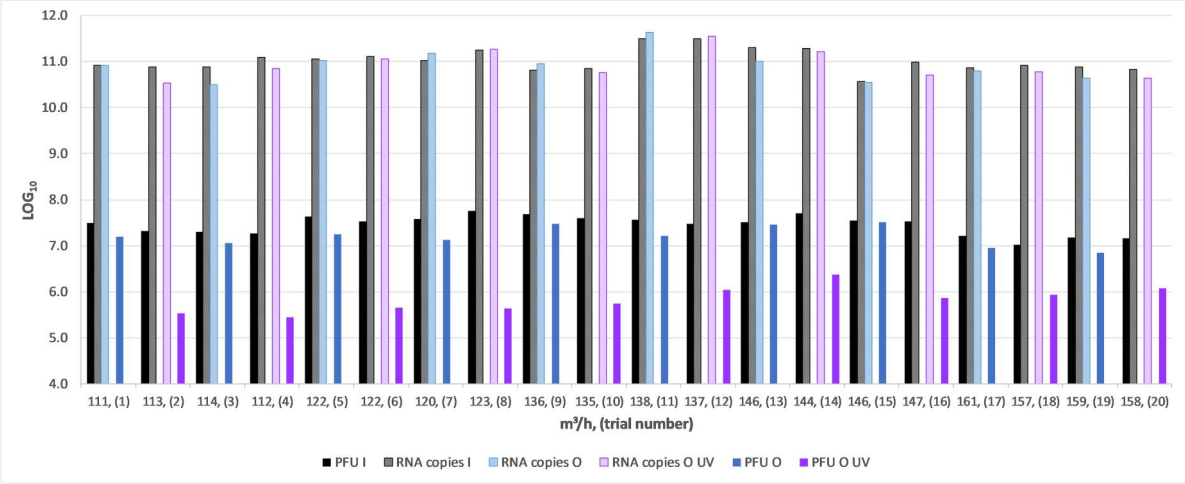

Figure 5. Concentrations (LOG_{10}/m^3) at different air flows. Shown are the number of airborne RNA copies and PFU at the inlet (I) and outlet (O). Concentrations at the outlet at active UV-C irradiation are marked with UV in the figure legend.

Table 2. Average concentrations and standard deviation (LOG_{10}/m^3) at the inlet (I) and outlet (O) at non-active and active UV-C irradiation (UV).

Variable	Arithmetic average	Standard deviation
PFU I	7.47	0.17
PFU I UV	7.43	0.22
PFU O	7.21	0.21
PFU O UV	5.83	0.27
RNA copies I	10.98	0.25
RNA copies I UV	11.07	0.21
RNA copies O	10.92	0.32
RNA copies O UV	10.93	0.31

The recorded concentrations exhibited a normal distribution (Shapiro-Wilk test, all P-values > 0.15). Average concentrations and standard deviations are presented in Table 2. The outlet's average concentrations were generally lower, and in cases of PFU I and PFU O compared to PFU O UV, a reduction of > 1 LOG_{10} PFU/m^3 was observed.

Samples taken simultaneously at the device's inlet and outlet were tested for significant differences using the paired T-test. Table 3 details the results of the paired T-test, revealing significant differences in PFU between the inlet and outlet. Nonetheless, the difference in RNA copies was only significantly different from zero when UV-C was activated. Conversely, PFU was also notably reduced when UV-C was deactivated, suggesting a varied foundational population of the two variables. There was no significant correlation ($p \geq 0.05$, Kendall's τ) between PFU and RNA copy numbers, indicating no significant dependency between these variables.

UV-C irradiation and residence time for particles in the irradiated sections of the device

The UV-C irradiations measured near the surface of one channel were 122 W/m^2 at the beginning, 139 W/m^2 in the middle and 21 W/m^2 at the end. The average was 94 W/m^2 (9.4 mW/cm^2), representing the estimated minimum exposure for a virus particle. Given that particles flow through two identical channels equipped with similar UV-C lamps, it is reasonable to assume that the irradiation in the second channel mirrors the first. However, the third channel lacked a UV lamp. For dose calculations, we factored in the modeled residence time for the irradiated channels. The residence times for particles, derived from modeled trajectories relative to the volume of passed air, are presented in Table 4. As the effective dose is proportional to residence time, quickly moving particles dictate the necessary timeframe for accurate dose estimation. Thus, the minimum required dose for virus particle exposure was ascertained from the 1st percentile of particle residence times while traversing the irradiated channels of the device. Please refer to Figure 3 for the corresponding deduced function.

The resulting residence times of particles at all times are cumulated by flow rate to form a discrete probability distribution, as displayed in Figure 6a for the flow rate of $\dot{V} = 150\,\frac{m^3}{h}$, where the number of samples in each bin is normalized with the total number of samples. The probability distributions for all flow rates are shown in Figure 6b, where it can be seen that—as was expected—the whole distribution shifts to lower residence times with increasing flow rate.

The dashed lines in Figure 6a demonstrate that both average and median residence times are largely ineffective for interpreting this data due to considerable positive skewness in the distributions. Furthermore, the bulk residence time, defined by $t_{bulk} = \frac{V_{irradiated}}{\dot{V}}$, i.e., the ratio of the volume of the irradiated channels and the flow rate vastly overestimates the residence time for most particles. Note that all characteristic numbers

Table 3. Results of the paired T-test to analyze significant differences between simultaneously taken samples at the inlet and outlet of the UV-C device.

Variable 1	Variable 2	Average of difference	Standard deviation	95% confidence interval	P-value
PFUI	PFUO	0.2636	0.1351	0.1670–0.3603	0.0002
PFUIUV	PFUOUV	1.6034	0.3526	1.3512–1.8556	< 0.0001
RNAI	RNAO	0.0615	0.1931	−0.0766–0.1996	0.3400
RNAIUV	RNAOUV	0.1352	0.1278	0.0437–0.2266	0.0086

Table 4. Modeled residence time of particles depending on air volumes passing the UV-C irradiated channels of the device.

	Residence time [s]			
$\dot{V}\left[\frac{m^3}{h}\right]$	1st particle	1st percentile	Mean	Median
100	0.3146	0.3509	0.7339	0.6179
150	0.2122	0.2378	0.4864	0.4075
200	0.1526	0.1774	0.3694	0.3156
250	0.1268	0.1442	0.2890	0.2424
300	0.1095	0.1206	0.2448	0.2101

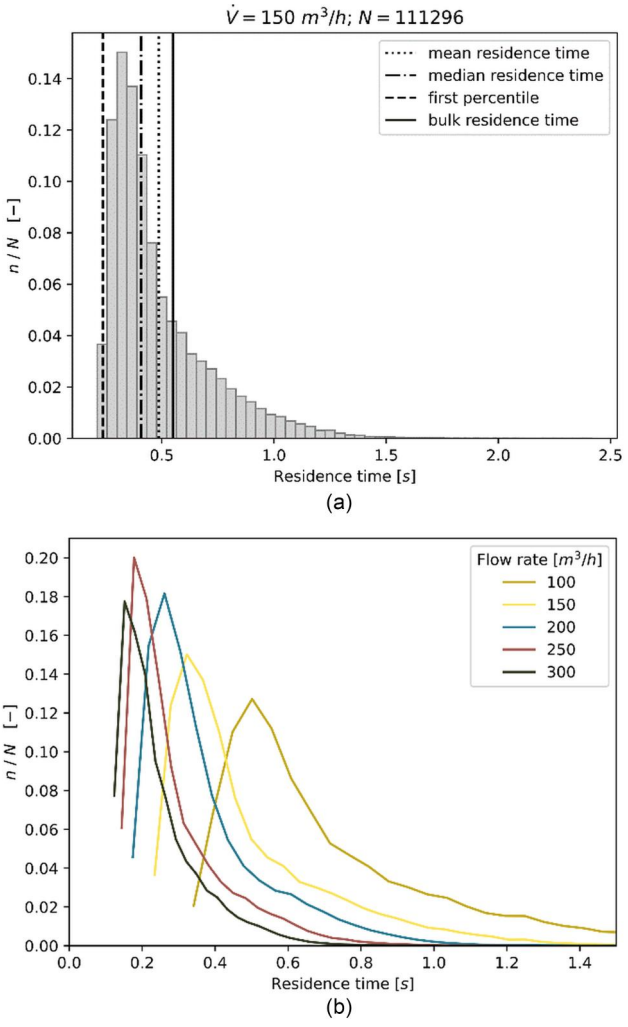

Figure 6. Residence times of particles in the irradiated channels of the device extracted from the flow simulations. (a) Normalized histogram of the residence times of particles in the irradiated channels of the device for $\dot{V} = 150\frac{m^3}{h}$. (b) Normalized probability distributions for all flow rates.

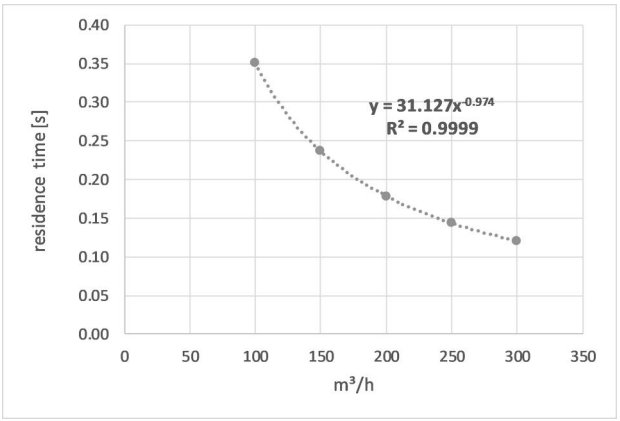

Figure 7. Residence time versus flow rate calculated by the 1st percentile of determined particle residence times. The function y = f (x) of the hyperbola and the coefficient of determination are shown in the diagram.

of Figure 6 are further summarized in Table 4, and the findings and insights are further elaborated below in the Discussion section. Consequently, we selected the significant residence time as the longest time in the 1st percentile. This choice means that if the device's UV radiation power is high enough to inactivate a virus particle within this timeframe, it is likely to inactivate 99% of incoming virus particles.

The device's residence time, in comparison with the traversing air volumes, exhibited a strong correlation and resulted in a power function (Figure 7).

The function $[s] = 31.127 * x^{-0.974}$, when multiplied with the recorded UV-C irradiance, provided the UV-C activated doses relative to adjusted air volumes (Equation (3) and Table 5).

$$\text{Dose}\left[\text{mWs/cm}^2\right] = \text{Residence time [s]} * 9.4\ \text{mW/cm}^2 \quad (3)$$

Table 5 shows the estimated minimum doses for 99% of airborne virus particles, as determined using the maximum distances from the UV-C lamp to UV-C sensor positions within the device. These calculations were instrumental in analyzing the correlation between the doses and reduction of cultivatable viruses (Table 6). Spearman's ρ correlation coefficient was found to be 0.77 ($p = 0.0092$), and Kendall's τ correlation was 0.60 ($p = 0.0157$), suggesting a strong

dependency between these variables. Every measured dose resulted in over 91% reduction, with some reaching as high as 99%. The trend showed that as the doses decreased, so did the level of reduction. However, reductions varied, indicating the influence of other factors. As seen in Tables 2 and 3, a significant reduction in PFU was observed when the UV-C was inactive, while no significant change in RNA copy numbers was observed between the inlet and outlet when the UV-C was switched off. Influencing factors will be discussed further.

Discussion

Commercially available air cleaners and prototypes are typically not designed for laboratory research. However, investigating their efficiency in realistic usage conditions is crucial. The prototype analyzed in this study was observed at standard room temperatures and moderate relative humidity, similar to what one might find in offices or healthcare facilities. The design of this prototype was not entirely suitable for studying particle effects, as expected turbulences could have occurred due to its internal structures (e.g., metal sheets, fixed irradiators). This is distinctly different from laboratory studies that measure bioaerosols in a laminar flow field, for example, Zhen et al. (2014).

In the conducted study, it was noticed that a significant natural loss of virus particles occurred when the viruses transited the device without UV-C irradiation.

Table 5. Calculated UV-C minimum doses for 99% of particles at adjusted air flows.

Sample no. (UV-C active)*	$\dot{V}\left[\frac{m^3}{h}\right]$	Dose [mWs/cm^2]
2	113	2.93
4	112	2.95
6	122	2.72
8	123	2.70
10	135	2.46
12	137	2.43
14	144	2.31
16	147	2.27
18	157	2.13
20	158	2.11

*No doses for samples with odd numbers because UV-C was inactive.

This observation stressed the importance of measuring virus load before it enters a device to ensure accurate interpretation of results. Although Knaus, Vatter, and Hessling (2021) implemented a different test setup to measure the UV-C effects on airborne viruses, they also recorded a loss of bioaerosols when UV-C was deactivated. The cause of this loss was not easily identifiable but was accounted for in their findings.

Regarding the present study, the air was streamlined prior to reaching the sampling sites and the magnitude of loss *via* the sampling technique is assumed to be relative. Concerning impaction, it can be mostly ruled out due to the nanometer scale of the nebulized viruses (Uhde et al. 2022). Regrettably, we were unable to measure nanometer particles at both the inlet and the outlet of the test system, which might be considered as one of this study's limitations. Factors such as agglomeration and electro-precipitation may have contributed to the natural loss of virus particles in the device. These are mere speculations, and the actual reasons remain unknown.

One essential consideration is that virus particles residing in the irradiated section of the system would have had to endure considerably higher UV-C doses. On the off chance some particles crossed into the third, non-irradiated section, those particles had already traveled through the irradiated section. The survival rate would be quite low. A case in point is the comparison between average concentrations at the outlet PFU O (7.21 LOG_{10} PFU/m^3) and PFU O UV (5.83 LOG_{10} PFU/m^3), where a reduction of 95.8% was observed. Hence, it is safe to infer that over 90% unaccounted virus fraction would have been inactivated by UV-C while crossing the system *via* the airborne route. Given this, any significant effect on the reduction efficiency of UV-C could be neglected.

The primary aim of the study was to assess the efficacy of a UV-C device in reducing airborne surrogate viruses, using phage MS2 as an example. This small virus surrogate is frequently studied and is often used as a surrogate for rhinoviruses. As stated in the introduction, the published D_{90} and D_{99} values for UV-C

Table 6. Reduction of airborne viruses relative to minimum doses.

Dose [mWs/cm^2]	Measured PFU IUV [LOG10/m^3]	Measured PFU OUV [LOG10/m^3]	Total reduction
2.93	7.32	5.53	98.37
2.95	7.26	5.44	98.50
2.72	7.52	5.66	98.64
2.70	7.75	5.64	99.23
2.46	7.61	5.75	98.62
2.43	7.48	6.04	96.36
2.31	7.69	6.37	95.24
2.27	7.52	5.87	97.76
2.13	7.02	5.93	91.88
2.11	7.16	6.08	91.75

irradiated viruses are useful for comparative purposes. Under the selected test conditions, the total reduction in viruses due to UV-C irradiation varied between 92% and 99%, resulting in equivalent D_{90} and D_{99} values. Viral reduction was noted to decrease with increased airflow, a result of the reduced UV-C dosage due to decreased residence time.

To determine the minimum exposure to viruses within the device, UV-C measurements were conducted in the prototype, providing an estimation of the minimum residence time required for 99% of virus particles. This conservative approach was designed to ensure the effectiveness of UV-C on bioaerosols. The UV-C irradiation was measured within the prototype at room temperature with a constant airflow. The output of UV-C from mercury low-pressure lamps can be affected by temperature fluctuations (Lau et al. 2012). As air exchange rates increased for the tests, temperatures in the UV-C irradiated section may have declined at higher air volumes. However, the recorded temperatures at the system's outlet during UV-C irradiation showed a standard deviation of ±1.3 °C, leading us to anticipate no significant impact on calculated dosage (Lau et al. 2012).

The model used to calculate particle residence times showed a reduced time of approximately one-third when comparing the lowest and highest airflows. Calculated doses dropped by about 28%, while the corresponding numbers of PFU decreased by around 6%. This study found higher doses were needed for effective MS2 virus inactivation than the ones cited in the introduction. The doses and reduction efficiency in the current investigation correlate well despite minor fluctuations, which may be due to methodological factors. One question that arises is whether the study doses may have been overestimated.

For instance, if the modeled residence time is compared to the 147 m^3/h air exchange rate (sample No. 16), the exchanged air volume would theoretically be 40.8 L per second. Considering the volume capacity of the two irradiated channels is 22.5 L, the full air changeover would take 0.55 s. This is a longer residence time than the modeled average of 0.47 s, possibly on account of pathlines with high velocities (Figure 4). This led us to suggest that estimating residence time *via* flow rate and device volume could result in an overestimation for virus particles, thereby leading to inflated calculated doses.

Tseng and Li (2005) employed air exchange to calculate exposure time and used a single sensor to gauge average facial intensity. The photon density diminishes with distance from the source, and photon output varied over the low-pressure mercury lamps' length (Lau et al. 2012). Utilizing average facial intensity may not accurately depict the average doses exposed to the viruses. The computed low doses from 0.8 to 0.9 mW s/cm^2 required to inactivate 99% of the airborne MS2 virus contradicts findings by Walker and Ko (2007). They found that about 31% of the MS2 virus remained infectious at 2.6 mW s/cm^2. An attempt was made to measure irradiation using AGI-30 impingers for PFU detection. This method mirrors the current study, but the dose needed for a nearly two-thirds reduction was greater than the D_{90} values in Table 5. A minimum dose of ≥2.1 mW s/cm^2 was adequate to inactivate over 90% of the virus, and the D_{99} value could potentially be expected at doses higher than 2.7 mW s/cm^2. UV-C irradiation measurements considered different photon densities across the length of the irradiators. However, the three sensor positions and sensor orientation probably missed reflecting photons from the stainless steel surface, which has a UV-C reflectance ratio of 24.5%, for example, Endo et al. (2021). Consequently, the calculated doses for the prototype might have been slightly underestimated. On the other hand, Snelling et al. (2022) measured UV-C irradiation precisely and found a requirement of 20 J/m^2 (equivalent to 2 mWs/cm^2) to inactivate 90% of airborne MS2, which aligns with our findings. We conclude that the prototype's dosage is adequate to effectively inactivate various airborne infectious viruses at all tested airflows. For instance, SARS-CoV-2 requires significantly lower doses (0.28 mWs/cm^2) for a reduction of >99% (Garg et al. 2023). The airborne influenza A virus is also susceptible to UV-C irradiation, reducing by 98.2% at maximum doses of 1.5 mW s/cm^2 (McDevitt, Rudnick, and Radonovich 2012). A high inactivation rate (>99%) is desirable for airborne viruses in general. Based on these findings, it is suggested that commercial devices based on this prototype operate at lower flow rates (below 135 m^3, for instance) to ensure high reduction rates. In this context, it should be considered that airborne viruses in mucus droplets (e.g., SARS-CoV-2) or in fecal particles (e.g., Highly Pathogenic Avian Influenza) could be less susceptible to UV-C irradiation. Unfortunately, data about that are scarce. Hill, Doughty, and Mackowski (2024) tested the effectivity of UV-C (222 nm and 254 nm) on SARS-CoV-2 in host particles. The average survival fraction in mucus particles irradiated with 2 mWs/cm^2 (254 nm) was less than 10%. Hence, it can be assumed that the tested prototype in the present study would reduce more than 90% of the virus in aerosols from humans.

In future, it would be interesting to compare the efficiency of the UV-C device with other types of air cleaners and to estimate the clean air delivery rate (CADR). Data of CADR from different air cleaning devices tested with the same surrogate (MS2) and the same detection method (all glass impinger, AGI.30) are available (Beswick et al. 2023). Further, the usefulness of UV-C irradiation should be taken into account. An advantage of using UV-C (254 nm) could be the reduced noise compared to HEPA filters and that no toxic or oxidizing compounds (HO, O_3) are released into the air when ozone free irradiators are used. An alternative to inactivate airborne viruses with 254 nm irradiators could be the use of excimer lamps with 222 nm. These lamps can be operated in rooms without inducing acute reactions in the skin or eyes of humans (Eadie et al. 2022). However, under discussion is the production of levels of ozone, OH radicals, and secondary organic species by excimer lamps which may have negative health impacts and should be ideally mitigated (Barber et al. 2023).

The non-irradiated RNA copy numbers detected by RT-PCR were 3.6 and 3.7 logs higher than the corresponding PFU count. Dreier, Störmer, and Kleesiek (2005) recorded a 2 LOG_{10} discrepancy between PFU per ml and RNA copies per ml in an MS2 stock solution. For air filter samples, the difference between PFU and copy numbers generally fell between 2 LOG_{10} and 5 LOG_{10} as shown in Bild 3 (means Figure 3) of an article from a German journal (Dreier et al. 2008). This discrepancy could be attributed to the presence of RNA fragments and incomplete virus particles in the nebulized suspension.

During virus production for virus isolation from the bacterial solution, some viruses were not fully formed, and some infected cells died before the virus production was completed. The detected RNA fragment (60 bp) was quite small, implying that RT-PCR could still detect partially synthesized RNA strands.

Notably, no significant correlation was observed between RNA copy numbers and respective PFU at the sampling sites. The changing relationship between PFU and RNA in the stored solution cannot be ruled out. However, this consideration does not clarify why the RNA concentration between the system's inlet and outlet did not significantly differ, like the PFU count. A possible explanation is a variation in particle sizes, with virus and RNA fragments being smaller than complete viruses. Thus, the impact on PFU losses, stronger for larger particles, could be less for these smaller fragments.

A significant reduction in RNA copies was recorded following UV-C irradiation. Although significant, this decrease was notably less substantial compared to the difference in PFU. The probability of UV-C photo lesions occurring in a small region for RNA amplification is lower than in an entire RNA strand of an infectious virus particle. Therefore, the reduction in RNA copy numbers under activated UV-C was only 19% when comparing arithmetic means between inlet and outlet.

The substantial differences between RNA copy numbers and active viruses are not unique to the tested virus; they are also observed in cases of influenza viruses, for example, Brown et al. (2015). Nevertheless, during an infection, there can be significant variations in the exhaled concentrations of active viruses and RNA copy numbers among infected individuals (Fabian et al. 2008). Moreover, while the range of an infectious dose of viral particles may be known, RT-PCR analysis only provides information about total viral particles, not active viral particles (Nikitin et al. 2014). Therefore, modeling virus spread, or risk assessment based on RNA fragment detection without knowledge of the relation between active particles and copy numbers would be speculative and unsuitable for such applications. Estimations based on viral RNA recovery could become even more complex when environmental factors affect both virus tenacity and nucleic acid detection as shown by Richter et al. (2023) who exposed SARS CoV-2 by heat. Surveillance and/or disinfection testing using RT-qPCR analysis may overestimate the presence of residual infectious virus (Hardison et al. 2022). Our study has shown, that degradation of irradiated RNA did not align with the loss of PFU. Desiccation, sunlight, and oxidation processes are examples of such factors in a natural environment.

Acknowledgements

HH and ML acknowledge the partial support of the research by the Helmholtz CORAERO (Airborne Transmission of SARS-CoV-2) project. Additional support is acknowledged from the Karlsruhe Institute of Technology, the Institute of Nanotechnology, and the Joint Research Laboratory Nanomaterials at TU Darmstadt. Further, we want to thank Kira Butenholz and Kevin Böttcher for their support during the measurements.

Authors contribution

Conceptualization, JS, JK, ML, HH; Laboratory analysis and measurements, VNL, ML; Data analysis JS, VNL, SB, AS, data curation, JS, VNL, SB, AS, JK and HH; Funding HH; Project administration HH, JS and NK; Writing – original

draft JS, SB, AS, JK, HH, NK; Writing – review & editing all authors. All authors have read and agreed to the published version of the manuscript.

Disclosure statement

No potential conflict of interest was reported by the author(s).

References

Abkar, L., K. Zimmermann, F. Dixit, A. Kheyrandish, and M. Mohseni. 2022. COVID-19 pandemic lesson learned-critical parameters and research needs for UVC inactivation of viral aerosols. *J. Hazard. Mater. Adv.* 8:100183. doi: 10.1016/j.hazadv.2022.100183.

Ahrens, J. P., B. Geveci, and C. C. Law. 2005. ParaView: An end-user tool for large-data visualization. In *The visualization handbook*, eds. C. D. Hansen and C. R. Johnson, 717–731. Burlington: Butterworth-Heinemann.

Allen, G. R., K. Benner, and W. P. Bahnfleth. 2021. Inactivation of pathogens in air using ultraviolet direct irradiation below exposure limits. *J. Res. Natl. Inst. Stand. Technol.* 126:126052. doi: 10.6028/jres.126.052.

Barber, V. P., M. B. Goss, L. J. F. Deloya, L. N. LeMar, Y. Li, E. Helstrom, M. Canagaratna, F. N. Keutsch, and J. H. Kroll. 2023. Indoor air quality implications of germicidal 222 nm light. *Environ. Sci. Technol.* 57 (42): 15990–8. doi: 10.1021/acs.est.3c05680.

Beswick, A., J. Brookes, I. Rosa, C. Bailey, C. Beynon, S. Stagg, and N. Bennett. 2023. Room-based assessment of mobile air cleaning devices using a bioaerosol challenge. *Appl. Biosaf.* 28 (1):1–10. doi: 10.1089/apb.2022.0028.

Bhardwaj, J., S. Hong, J. Jang, C.-H. Han, J. Lee, and J. Jang. 2021. Recent advancements in the measurement of pathogenic airborne viruses. *J. Hazard. Mater.* 420: 126574. doi: 10.1016/j.jhazmat.2021.126574.

Brown, J. R., J. W. Tang, L. Pankhurst, N. Klein, V. Gant, K. M. Lai, J. McCauley, and J. Breuer. 2015. Influenza virus survival in aerosols and estimates of viable virus loss resulting from aerosolization and air-sampling. *J. Hosp. Infect.* 91 (3):278–81. doi: 10.1016/j.jhin.2015.08.004.

Buonanno, G., A. Robotto, E. Brizio, L. Morawska, A. Civra, F. Corino, D. Lembo, G. Ficco, and L. Stabile. 2022. Link between SARS-CoV-2 emissions and airborne concentrations: Closing the gap in understanding. *J. Hazard. Mater.* 428:128279. doi: 10.1016/j.jhazmat.2022.128279.

Cox, J., H. Mbareche, W. G. Lindsley, and C. Duchaine. 2020. Field sampling of indoor bioaerosols. *Aerosol Sci. Technol.* 54 (5):572–84. doi: 10.1080/02786826.2019.1688759.

Dreier, J., A. Bermpohl, P. Jeschin, B. Becker, and K. Kleesiek. 2008. Transmission von Viren durch Raumlufttechnische Anlagen und Inaktivierung durch UVC-Strahlung. *Gefahrstoffe - Reinhaltung Der Luft* 68:379–83.

Dreier, J., M. Störmer, and K. Kleesiek. 2005. Use of bacteriophage MS2 as an internal control in viral reverse transcription-PCR assays. *J. Clin. Microbiol.* 43 (9):4551–7. doi: 10.1128/jcm.43.9.4551-4557.2005.

Eadie, E., W. Hiwar, L. Fletcher, E. Tidswell, P. O'Mahoney, M. Buonanno, D. Welch, C. S. Adamson, D. J. Brenner, C. Noakes, et al. 2022. Far-UVC (222 nm) efficiently inactivates an airborne pathogen in a room-sized chamber. *Sci. Rep.* 12 (1):4373. doi: 10.1038/s41598-022-08462-z.

Endo, T., A. Gemma, R. Mitsuyoshi, H. Kodama, D. Asaka, M. Kono, T. Mochizuki, H. Kojima, T. Iwamoto, and S. Saito. 2021. Discussion on effect of material on UV reflection and its disinfection with focus on Japanese Stucco for interior wall. *Sci. Rep.* 11 (1):21840. doi: 10.1038/s41598-021-01315-1.

Fabian, P., J. J. McDevitt, W. H. DeHaan, R. O. Fung, B. J. Cowling, K. H. Chan, G. M. Leung, and D. K. Milton. 2008. Influenza virus in human exhaled breath: An observational study. *PLoS One.* 3 (7):e2691. doi: 10.1371/journal.pone.0002691.

Garg, H., R. P. Ringe, S. Das, S. Parkash, B. Thakur, R. Delipan, A. Kumar, K. Kulkarni, K. Bansal, P. B. Patil, et al. 2023. UVC-based air disinfection systems for rapid inactivation of SARS-CoV-2 present in the air. *Pathogens* 12 (3):419. doi: 10.3390/pathogens12030419.

Hardison, R. L., S. W. Nelson, R. Limmer, J. Marx, B. M. Taylor, R. R. James, M. J. Stewart, S. D. D. Lee, M. W. Calfee, S. P. Ryan, et al. 2022. Efficacy of chemical disinfectants against SARS-CoV-2 on high-touch surface materials. *J. Appl. Microbiol.* 134 (1):1–12. doi: 10.1093/jambio/lxac020.

Hill, S. C., D. C. Doughty, and D. W. Mackowski. 2024. Inactivation of virions in host particles in air using 222- and 254-nm UV: Dependence of shielding on particle size and UV wavelength. *Aerosol Sci. Technol.* 58 (5):512–35. doi: 10.1080/02786826.2024.2314614.

Jensen, M. M. 1964. Inactivation of airborne viruses by ultraviolet irradiation. *Appl. Microbiol.* 12 (5):418–20. doi: 10.1128/am.12.5.418-420.1964.

Knaus, J., P. Vatter, and M. Hessling. 2021. Development and Verification of a Test Rig for Inactivation of Bacteria and (Corona-) Viruses by Uvc Air Disinfection Systems. *Current Directions in Biomedical Engineering* 7 (2):315–8. doi: 10.1515/cdbme-2021-2080.

Kowalski, W. 2010. *Ultraviolet germicidal irradiation handbook: UVGI for air and surface disinfection*. Berlin Heidelberg: Springer.

Lau, J., W. Bahnfleth, R. Mistrick, and D. Kompare. 2012. Ultraviolet irradiance measurement and modeling for evaluating the effectiveness of in-duct ultraviolet germicidal irradiation devices. *HVAC&R Research* 18 (4):626–42. doi: 10.1080/10789669.2011.611575.

McDevitt, J. J., S. N. Rudnick, and L. J. Radonovich. 2012. Aerosol susceptibility of influenza virus to UV-C light. *Appl. Environ. Microbiol.* 78 (6):1666–9. doi: 10.1128/aem.06960-11.

Menter, F., M. Kuntz, and R. B. Langtry. 2003. Ten years of industrial experience with the SST turbulence model. *Turbulence Heat Mass Transfer* 4:625–32.

Montalli, V. A. M., P. R. Freitas, M. F. Torres, O. F. Torres Junior, D. H. M. Vilhena, J. L. C. Junqueira, and M. H. Napimoga. 2021. Biosafety devices to control the spread of potentially contaminated dispersion particles. New associated strategies for health environments. *PLoS One.* 16 (8):e0255533. doi: 10.1371/journal.pone.0255533.

Nikitin, N., E. Petrova, E. Trifonova, and O. Karpova. 2014. Influenza virus aerosols in the air and their

infectiousness. *Adv. Virol.* 2014:859090. doi: 10.1155/2014/859090.

OpenCFD Limited. 2021. OpenFOAM v2112 user guide. https://www.openfoam.com/documentation/guides/v2112/doc/index.htm

Richter, W., M. Sunderman, D. Schaeufele, Z. Willenberg, K. Ratliff, M. Calfee, and L. Oudejans. 2023. Evaluation of steam heat as a decontamination approach for SARS-CoV-2 when applied to common transit-related materials. *J. Appl. Microbiol.* 134 (3):1–9. doi: 10.1093/jambio/lxad053.

Shen, J., M. Kong, B. Dong, M. J. Birnkrant, and J. Zhang. 2021. Airborne transmission of SARS-CoV-2 in indoor environments: A comprehensive review. *Science and Technology for the Built Environment* 27 (10):1331–67. doi: 10.1080/23744731.2021.1977693.

Snelling, W. J., A. Afkhami, H. L. Turkington, C. Carlisle, S. L. Cosby, J. W. J. Hamilton, N. G. Ternan, and P. S. M. Dunlop. 2022. Efficacy of single pass UVC air treatment for the inactivation of coronavirus, MS2 coliphage and *Staphylococcus aureus* bioaerosols. *J. Aerosol Sci.* 164:106003. doi: 10.1016/j.jaerosci.2022.106003.

Spurk, J. H., and N. Aksel. 2020. *Fluid mechanics* (3rd ed.). Berlin Heidelberg: Springer.

Szczotko, M., I. Orych, M. Łukasz, and J. Solecka. 2022. A review of selected types of indoor air purifiers in terms of microbial air contamonation reduction. *Atmospere* 13 (5):800. doi: https://doi.org/10.3390/atmos13050800.

Tseng, C., and C. Li. 2008. Inactivation of surface viruses by gaseous ozone. *J. Environ. Health.* 70 (10):56–62.

Tseng, C.-C., and C.-S. Li. 2005. Inactivation of virus-containing aerosols by ultraviolet germicidal irradiation. *Aerosol Sci. Technol.* 39 (12):1136–42. doi: 10.1080/02786820500428575.

Uhde, E., T. Salthammer, S. Wientzek, A. Springorum, and J. Schulz. 2022. Effectiveness of air-purifying devices and measures to reduce the exposure to bioaerosols in school classrooms. *Indoor Air.* 32 (8):e13087. doi: 10.1111/ina.13087.

Volkoff, S. J., T. J. Carlson, K. Leik, J. J. Smith, D. Graves, P. Dennis, T. Aris, D. Cuthbertson, A. Holmes, K. Craig, et al. 2021. Demonstrated SARS-CoV-2 Surface Disinfection Using Ozone. *Ozone: Science & Engineering* 43 (4):296–305. doi: 10.1080/01919512.2020.1863770.

Walker, C. M., and G. Ko. 2007. Effect of ultraviolet germicidal irradiation on viral aerosols. *Environ. Sci. Technol.* 41 (15):5460–5. doi: 10.1021/es070056u.

Weller, H. G., G. Tabor, H. Jasak, and C. Fureby. 1998. A tensorial approach to computational continuum mechanics using object-oriented techniques. *Computer in Physics* 12 (6):620–31. doi: 10.1063/1.168744.

Yang, Y., H. Zhang, S. S. Nunayon, V. Chan, and A. C. Lai. 2018. Disinfection efficacy of ultraviolet germicidal irradiation on airborne bacteria in ventilation ducts. *Indoor Air.* 28 (6):806–17. doi: 10.1111/ina.12504.

Zhen, H., T. Han, D. Fennell, and G. Mainelis. 2014. A Systematic Comparison of Four Bioaerosol Generators: Affect on Culturability and Cell Membrane Integrity when Aerosolizing Escherichia coli Bacteria. *J. Aerosol Sci.* 70:67–79. doi: 10.1016/j.jaerosci.2014.01.002.